Geomechanics and Engineering, *Vol. 31, No. 3 (2022) 237-248*
https://doi.org/10.12989/gae.2022.31.3.237

Three-dimensional numerical parametric study of shape effects on multiple tunnel interactions

Li'ang Chen[1a], Weiwei Pei[2b], Yihong Yang[2c] and Wanli Guo*[3]

[1]*Guangzhou Metro Design&Research Institute Co.,Ltd., Guangzhou, Guangdong, P. R. China*
[2]*Wenzhou Design Assembly Company Ltd, Wenzhou 325000, China*
[3]*Geotechnical Engineering Department, Nanjing Hydraulic Research Institute, Nanjing 210024, China*

(*Received August 8, 2022, Revised September 15, 2022, Accepted October 18, 2022*)

Abstract. Nowadays, more and more subway tunnels were planed and constructed underneath the ground of urban cities to relieve the congested traffic. Potential damage may occur in existing tunnel if the new tunnel is constructed too close. So far, previous studies mainly focused on the tunnel-tunnel interactions with circular shape. The difference between circular and horseshoe shaped tunnel in terms of deformation mechanism is not fully investigated. In this study, three-dimensional numerical parametric studies were carried out to explore the effect of different tunnel shapes on the complicated tunnel-tunnel interaction problem. Parameters considered include volume loss, tunnel stiffness and relative density. It is found that the value of volume loss play the most important role in the multi-tunnel interactions. For a typical condition in this study, the maximum invert settlement and gradient along longitudinal direction of horseshoe shaped tunnel was 50% and 96% larger than those in circular case, respectively. This is because of the larger vertical soil displacement underneath existing tunnel. Due to the discontinuous hoop axial stress in horseshoe shaped tunnel, significant shear stress was mobilized around the axillary angles. This resulted in substantial bending moment at the bottom plate and side walls of horseshoe shaped tunnel. Consequently, vertical elongation and horizontal compression in circular existing tunnel were 45% and 33% smaller than those in horseshoe case (at monitored section X/D = 0), which in latter case was mainly attributed to the bending induced deflection. The radial deformation stiffness of circular tunnel is more sensitive to the Young's modulus compared with horseshoe shaped tunnel. This is because of that circular tunnel resisted the radial deformation mainly by its hoop axial stress while horseshoe shaped tunnel do so mainly by its flexural rigidity. In addition, the reduction of soil stiffness beneath the circular tunnel was larger than that in horseshoe shaped tunnel at each level of relative density, indicating that large portion of tunneling effect were undertaken by the ground itself in circular tunnel case.

Keywords: shape; three-dimensional numerical analysis; tunnel stiffness; volume loss

1. Introduction

Underground space is becoming more and more congested in cosmopolitan cities due to the economic development. As a result, underground infrastructures (e.g., tunnels) might be constructed with closer and closer distance. Specifically, when existing tunnel is experiencing nearby new tunnel constructions, stress redistribution may be induced in surrounding soils. This might further cause adverse effects such as cracks to existing tunnel (Cooper *et al.* 2002). Thus, the response of existing tunnel subjected to new tunnel construction is needed to be investigated for estimating potential damage of existing tunnel and taking remedial measured if necessary.

To investigate this tunnel-tunnel interaction problem, two major approaches have been adopted in recent years: field monitoring (Mohamad *et al.* 2010, Mohamad *et al.* 2012, Li and Yuan 2012, Eskandari *et al.* 2018, Shi *et al.* 2020, Shi *et al.* 2022a), physical tests (Ng *et al.* 2013, Kim *et al.* 1998, Fang *et al.* 2022, Shi *et al.* 2022b). However, it is difficult for those results to be widely applied due to the variations in ground condition, tunnel stiffness and workmanship of new tunnel excavation (e.g., volume loss) in reality. Alternatively, numerical analysis (Liu *et al.* 2009, Nawel and Salah 2015, Yoo and Cui 2020) is more effective way to systematically analyze this complex interaction between tunnels because of its low cost and wide range of application.

Centrifuge tests and numerical simulations have been conducted to investigate the interactions between existing tunnel and new perpendicularly crossing tunnel(s) (Ng *et al.* 2013a, Ng *et al.* 2015, Boonyarak and Ng 2014). The effects of pillar depth, tunnel shielding, cover depth and construction sequence were considered. Some researches focus on the effects of stratigraphic uncertainty and soil spatial variability on soil-tunnel interaction (Shi and Wang 2021, Wang *et al.* 2022).

Attentions have been paid on Enhancing the soil property by bio-inspired soil reinforcement technology, which might mitigate the tunnelling induced excessive soil movement (Bai *et al.* 2021, Hu *et al.* 2021, Wang *et al.* 2022). The effect of blast loading on urban rock tunnel with

*Corresponding author, Ph.D. Senior Engineer
E-mail: guowljs@163.com
[a]MPhil
[b]MPhil

ISSN: 2005-307X (Print), 2092-6219 (Online)

considering rock weathering was investigated by former studies (Zaid *et al.* 2022, Mishra *et al.* 2022, Sadique *et al.* 2022, Zaid and Shah 2021, Zaid 2021a, b, c, Zaud and Mishara 2021).

As far as author is aware, no directly study has been carried out on the influence of different tunnel shapes on the existing tunnel. However, the different deformation mechanisms were observed between horseshoe shaped tunnel and circular tunnel (González *et al.* 2008) that horseshoe shaped tunnel always experience larger deformation. To address those issues mentioned above, extensive three-dimensional numerical parametric analyses were conducted to investigate the influence of tunnel shapes on crossing tunnel interactions. Verification of numerical morel is first conducted based on measured result from centrifuge test. Afterwards, a comparative numerical study with equivalent circular existing tunnel was conducted to investigate the difference in tunnel-tunnel interactions purely due to the change of existing tunnel shape. Afterwards, three-dimensional numerical parametric studies are conducted to investigate the shape effect on tunnel-tunnel interaction with considering different volume loss, tunnel stiffness and relative density.

2. Three-dimensional numerical modelling

The finite element program, Plaxis 3D, was adopted in this study to carry out three dimensional numerical analyses. A numerical back-analysis of reported centrifuge test (Jiang *et al.* 2015) investigating twin-tunnel excavation effect on existing tunnel was used as referenced test. Two different shapes of existing tunnel (i.e., horseshoe and circular) were modeled and considered in this study. By varying volume loss (tunneling induced volumetric soil loss around new tunnel), stiffness of existing tunnel and relative density of sand, a systematical numerical investigation on the complicated tunnel-tunnel interaction was conducted. Prior to the numerical parametrical studies, the reliability of adopted constitutive model and model parameters were examined by results from centrifuge test.

The reference three-dimensional centrifuge test was carried out at 60 g (60 times gravitational acceleration) in the Geotechnical Centrifuge Facility of the Hong Kong University of Science and Technology (Ng 2014). Figs. 1(a) and 1(b) show the centrifuge model setup of the referenced test. The dimension of model container is 1250 (length)×930 (width)×800(depth) mm, which is equivalent to 75×55.8×48 m in prototype. The longitudinal direction of existing tunnel was normal to those of new tunnels. The horizontal clearance between two new tunnels was 100 mm (equivalent to 6 m in prototype). The cover depth of existing tunnel and new tunnel were 73 and 470 mm, respectively. The pillar depth (vertical clearance) between existing tunnel and new tunnels was 200 mm (equivalent to 12 m in prototype). The new model tunnels were excavated in 12 steps along 'Y' direction, following the sequence of L1, L2…L6 and R1, R2…R6 shown in Fig. 1(a). The length of each excavation step is 60mm (equivalent to 3.6 m in prototype). The total excavation length is 21.6 m, which is

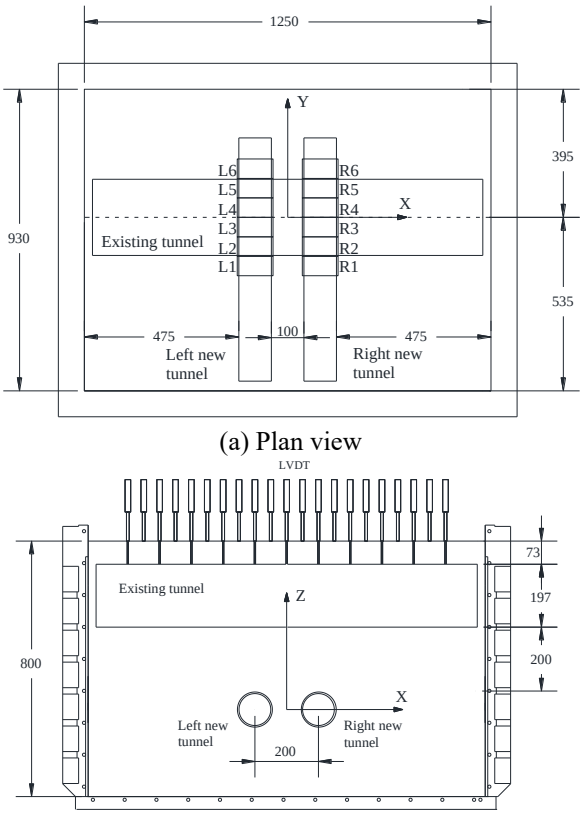

(a) Plan view

(b) Elevation view

Fig. 1 Schematic diagrams of centrifuge model package. (Dimensions in millimeters)

about 1.8 times the height of existing tunnel. The excavation length is long enough to study the deformation mechanism of different shape and sensitivity of parameters. Dry Toyoura sand was adopted in the centrifuge test. By using the sand pluvial deposition method (Ng *et al*. 2013a), relatively uniform sand sample was obtained. The average relative density (Dr) of sand sample in the test was 62%. Further detailed information about this centrifuge test was reported by (Jiang *et al.* 2015).

2.1 Numerical analysis program

The numerical analyses conducted in this study were summarized in Table 1.

In total, 14 numerical runs were performed. To obtain a comprehensive understanding of shape effect on multi-tunnel interaction, a series of parametric studies considering different volume losses, tunnel stiffness and sand relative densities were conducted. To study the sensitivity of volume loss (VL) on tunnel response, 3 values of new tunnel excavation induced volume loss were considered (i.e., 0.5%, 1.5% and 2.5%). The 0.5% of volume loss can be achieved in most cases nowadays by advanced EPB (Earth pressure balance) shield method. 1.5% and 2.5% of volume losses represent the conditions with average and poor construction control, respectively. To investigate the influence of existing tunnel stiffness on multiple tunnel interaction, 3 values of the Young's modulus of existing

Table 1 Summary of three-dimensional numerical parametric studies performed in this study

ID	Series	Shape of existing tunnel	Volume loss	modulus of existing tunnel (GPa)	Relative density of sand
1	Volume loss	Horseshoe	0.5%	69	62%
2		Horseshoe	1.5%		
3		Horseshoe	2.5%		
4		Circular	0.5%		
5		Circular	1.5%		
6		Circular	2.5%		
7	Tunnel stiffness	Horseshoe	1.5%	30	62%
8		Horseshoe		69	
9		Horseshoe		150	
10		Circular		30	
11		Circular		69	
12		Circular		150	
13	Relative density	Horseshoe	1.5%	69	30%
14		Horseshoe			62%
15		Horseshoe			90%
16		Circular			30%
17		Circular			62%
18		Circular			90%

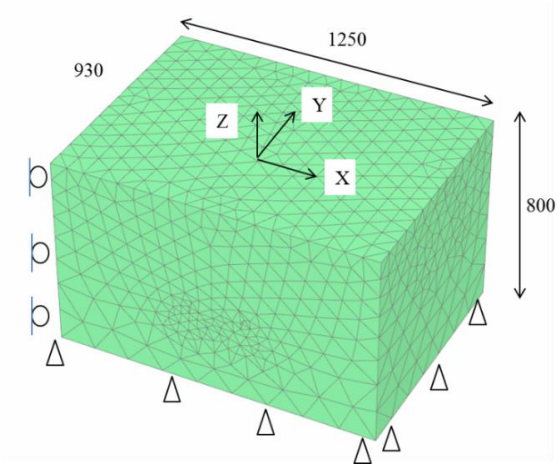

(a) Three-dimensional finite element mesh for numerical back-analysis

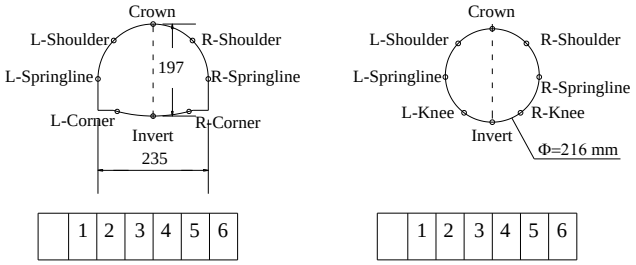

(b) Cross section view of monitoring section in back-analysis and comparative study

Fig. 2 Modelling of numerical analysis (Dimensions in millimeters)

tunnel were considered in this study (i.e., 30, 69 and 150 GPa). The 30, 69 and 150 GPa represent typical Young's modulus of concrete, aluminum and cast iron, respectively. Additionally, 3 relative densities of sand (i.e., 30%, 62% and 90%) were selected to explore the influence of relative density on tunnel-soil-tunnel interaction. In the test series of volume loss, direct comparison was made between two cases with horseshoe shaped and circular existing tunnel under VL= 1.5% condition (i.e., test 2 and test 5). Test 2 was essential numerical back-analysis of reference centrifuge test with horseshoe shaped existing tunnel. Test 5, whose existing tunnel was replaced by an equivalent circular tunnel, was the comparative study of test 2. The variety of excavation scale (i.e., size of new tunnel) is not considered in this study.

2.2 Finite element mesh and boundary conditions

Fig. 2(a) shows finite element meshes adopted in this study. Parameter studies on the mesh density have been conducted to ensure the accuracy of model. The dimension of soil model was 1250 mm (length) ×930 mm (width) ×800 mm (depth). A 10-node tetrahedral element was used to model the soil. The displacements perpendicular to the four vertical sides (i.e., left, right, front and rear) of the mesh were restricted. Pin support was applied to the base boundary of the mesh.

According to Table 1, total two types of numerical model are needed essentially, depending on the shape of existing tunnel. The rest of parametric studies were basically following the same numerical setup with test 2 or test 5 but with different model parameters (i.e., volume loss, tunnel stiffness and relative density). Fig. 2(b) shows the section views of existing tunnel in horseshoe shape and circular shape, corresponding to test 2 and test 5, respectively. The model geometry and tunnel position in test 2 was identical to that of centrifuge test (model scale). The width and height of horseshoe shaped tunnel is 235 and 197 mm, respectively. To make a fair comparison, circular existing tunnel was designed to have identical longitudinal and transverse flexural stiffness as horseshoe shaped tunnel. The diameter of circular tunnel is 216 mm. The thicknesses of tunnel lining in both cases are 6.5 mm. Additionally, the centroids of existing tunnels in both cases were kept in the same depth. The tunnel lining was modeled using 6-node elastic plate element since its thickness is relatively small compared with tunnel's size. Tie constraint was applied between tunnel lining and surrounding soil.

2.3 Constitutive model and model parameters

The constitutive model adopted in this study was the hypoplasticity model with small strain stiffness (Gudehus and Mašín 2009, Shi *et al*. 2015). Hypoplastic constitutive model was developed to describe nonlinear behavior of granular material (Von 1996). By incorporating the concept of intergranular strain, this constitutive model is able to capture the strain and stress path dependency of soil stiffness under small strain condition (Niemunis and Herle 1997, Shi *et al*. 2018). The common of soil-structure interaction problems is their stress redistribution mechanism, which involves complicated stress / strain history and loading path in soil. The constitutive model of

Table 2 Summary of material parameters adopted in the finite element analysis

$\varphi_c'^{a}$	Angle of internal shearing resistance at critical state	30°
h_s [a]	Hardness of granulates	2.6 GPa
n [a]	Exponent controls the shape of limiting void ratio curves	0.27
e_{do}[a]	Minimum void ratio at zero pressure	0.61
e_{co}[a]	Critical void ratio at zero pressure	0.98
e_{io}[a]	Maximum void ratio at zero pressure	1.10
α [b]	Exponent controls the dependency of peak friction angle on relative density	0.5
β [b]	Exponent controls the dependency of soil stiffness on relative density	3
m_R [b]	Parameter controlling initial shear modulus upon 180° strain path reversal	8
m_T [b]	Parameter controlling initial shear modulus upon 90° strain path reversal	4
R [b]	Elastic range	3×10-5
β_r [b]	Parameter controlling stiffness degradation rate with strain	0.2
χ [b]	Parameter controlling stiffness degradation rate with strain	1.0
K_0	Coefficient of at-rest earth pressure	0.5

hypoplasticity can well capture the above state variables theoretically, which means it is suitable for this study.

The physical meanings and adopted values of model parameters in this study were summarized in Table 2. This set of soil parameters has been successfully used to back-analyze their centrifuge test on tunnel-tunnel interaction problems (Ng *et al*. 2013a, Ng *et al.* 2015, Boonyarak and Ng 2014, Jiang *et al.* 2015, Shi *et al.* 2019).

In most of the numerical analyses, all the new tunnels and existing tunnel were modeled as linear elastic material with Young's modulus and Poisson's ratio of 69 GPa and 0.33, respectively. However, the Young's modulus of existing tunnel in some cases varied from 30 GPa to 150 GPa, which is shown in Table 1.

2.4 Numerical modeling procedures

Details of the numerical modeling procedures are listed as follows:

1. Established the initial boundary and stress conditions of soil at 1 g, define coefficient of at-rest earth pressure (K0) as 0.5. Activate the existing tunnel and new tunnels as wished-in-place.
2. Simulated the change of gravitational acceleration from 1g to 60 g by increasing the unit weight of soil and tunnel by 60 times. This step is to simulate the spin-up process of centrifuge.
3. Modeled each tunnel excavation step by simulating both volume loss and weight loss simultaneously. Weight loss was simulated by deactivate the soil inside the new tunnel. Volume loss was achieved by applying a uniform radial contraction to tunnel lining.
4. Repeat step 3 until 12 excavation steps of two new tunnels were finished.

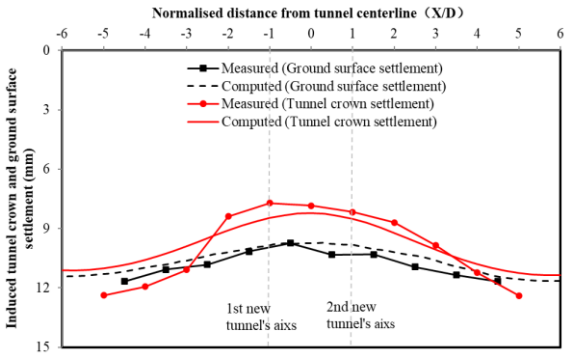

Fig. 3 Comparison of measured results with computed results of induced tunnel crown and ground settlement at the end of twin-tunnel excavation

3. Verfication of adopted numerical model

In this and following sections which are interpretation of results, all results would be presented in prototype scale unless stated otherwise. Moreover, existing tunnel response reached its peak value after twin-tunnel excavations were completed. For simplicity, only results after twin-tunnel excavations were finished are discussed. All the results (e.g., settlement) discussed in this manuscript is purely caused by adjacent new tunnel excavation rather than total response.

Fig. 3 shows the comparison between measured and computed results of existing tunnel crown and ground surface settlements. The results are selected at the stage when twin-tunnel excavations were completed. Settlement curve was plotted along existing tunnel's longitudinal direction. The diameter of new tunnel is used for normalizing the distance from existing tunnel midline. Both the measured and computed results showed that the existing tunnel crown and ground surface settled with hogging curve, which means tunnel crown and ground surface settle less at the middle. The reason of this phenomenon is beyond the scope of this study and already discussed by previous literature (Jiang *et al.* 2015). When the normalized distance from existing tunnel midline is larger than 3D, the computed settlements were less than the measured ones. This could be attributed to the difference in boundary conditions between centrifuge and numerical model. The frictions exist between model box and soil boundary while roller support was defined at vertical boundary in numerical model.

The maximum settlement and trend of numerical results show that the computed results matched the measured results well (less than 10% difference in average), especially in the region away from the boundary (i.e., -3< X/D< 3). Therefore, it can be concluded that the numerical model (constitutive model and modeling procedure) adopted in this study is reasonable.

4. Effect of volume loss on existing tunnel response

4.1 Maximum settlement and longitudinal bending strain of existing tunnel with variations of volume losses

Fig. 4(a) shows relationship between maximum settlements and settlement gradient of existing tunnel with volume loss caused by new tunnel excavation. In this study, volume loss varied from 0.5% to 2.5%. Invert settlement is larger than crown due to tunnel's vertical elongation. Moreover, its maximum value was located at middle of existing tunnel (X/D=0). Thus, the invert settlement of existing tunnel at X/D = 0 was selected and compared. As expected, as volume loss increased, maximum tunnel settlement increased, but at a reduced rate. This is because of that soil is unable to sustain tensile stress. The value of stress relief beneath the existing tunnel was limited by the original vertical stress. Therefore, with same amount of volume loss increased, the stress relief beneath the existing tunnel would increase with reducing rate. It is observed that maximum settlements of circular tunnel were 30-35% less than horseshoe shaped tunnel. With higher volume loss, the settlement difference between circular tunnel and horseshoe shaped tunnel became larger, indicating that the response of circular existing tunnel is less sensitive to volume loss. At volume loss of 1.5%, maximum invert settlement (22.8 mm) of horseshoe shaped tunnel already exceeded the allowable limit of 20 mm (BD 2009). However, even at volume loss of 2.5%, maximum invert settlement of circular tunnel (21.2) only exceeded limit by 6% (BD 2009). Maximum gradients of tunnel invert settlement were also plotted in Figure 4a. For circular existing tunnel case, the maximum gradient increased with increasing volume loss at a reducing rate. However, the horseshoe tunnel's maximum gradient increased almost linearly. This is perhaps due to the different positions of reverse bending points in two cases. The maximum gradients of horseshoe shaped tunnel were much larger than those of circular tunnel at each level of volume loss. At volume loss of 0.5% and 1.5%, maximum gradient of both horseshoe and circular tunnel were within the limit of 1/1000 (BD 2009, LTA 2000). When applied volume loss was 2.5%, horseshoe shaped tunnel's maximum gradient (1/630) exceeded the allowable limit, while the maximum gradient of circular tunnel (1/1763) was only about one third of that in horseshoe shaped tunnel. Countermeasures (e.g. grouting for shield tunnel) may be necessary to reduce the excessive tunnel settlement of horseshoe shaped tunnel induced by twin-tunnel excavation.

Fig. 4(b) shows the variation of maximum longitudinal bending strain at invert with volume loss induced by new tunnel excavation. The longitudinal bending strain on invert is equal to $(\Delta\varepsilon_{Invert} - \Delta\varepsilon_{Crown})/2$. The symbols $\Delta\varepsilon_{Invert}$ and $\Delta\varepsilon_{Crown}$ represent the incremental longitudinal strain at invert and crown of existing tunnel, respectively. The maximum longitudinal bending strain was located at middle of existing tunnel, between the centerline of 1st new tunnel and 2nd new tunnel. At volume loss of 0.5%, the maximum longitudinal bending strain in circular and horseshoe shaped tunnel were 14.5 and 12.5 με, respectively. Circular existing tunnel bore larger strain. When volume loss reached 1.5%, those values in two cases increased to 40.7 and 40.6 με, respectively. The maximum longitudinal bending strain in horseshoe shaped tunnel overtook that in circular tunnel a bit. However, when volume loss was further increased to 2.5%, the maximum longitudinal bending strain in horseshoe shaped tunnel (63.5 με) already exceeded that in circular tunnel (53.3 με) by 20%. It is clear that the increasing rate of longitudinal bending strain with volume loss is larger (about 30%) in horseshoe shaped tunnel in relative to circular tunnel. Consistent to the variation of maximum tunnel gradient, the maximum longitudinal bending strain of circular existing tunnel also increased with increasing volume loss at a reducing rate, while the horseshoe tunnel varied linearly. This illustrated that the longitudinal strain of horseshoe tunnel is highly relevant to the volume loss. Apart from this, the longitudinal bending strains in both cases were far less than the allowable tensile strain of unreinforced concrete of 150 με (ACI 2001), indicating that the stiffness of existing tunnel (including size, lining thickness and material modulus) relative to the new tunnel adopted in this study is high enough.

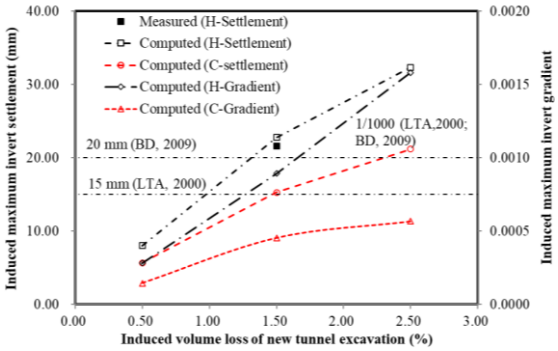

(a) Maximum tunnel invert settlement and settlement gradient

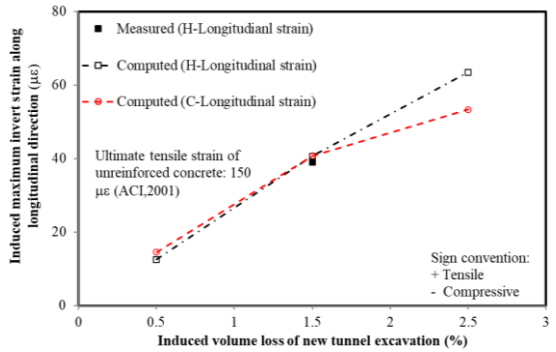

(b) Maximum longitudinal strain on invert

Fig. 4 Effect of induced volume loss on tunnel responses

All results of settlement, settlement gradient and longitudinal bending strain of existing tunnel demonstrated that horseshoe shaped tunnel suffered more dangerous serviceability issues in relative to circular tunnel with given condition in this study. In order to further explain why tunneling induced responses of horseshoe shaped existing tunnel are always larger than those in circular existing tunnel. Direct comparison and discussed was made between two cases with volume loss = 1.5% (i.e., test 2 and test 5) in next section. The only difference between test 2 and test 5 was the shape of existing tunnel. The results from test 2 and test 5 were marked with 'Horseshoe' and 'Circular', respectively. Fortunately, measured results are available in

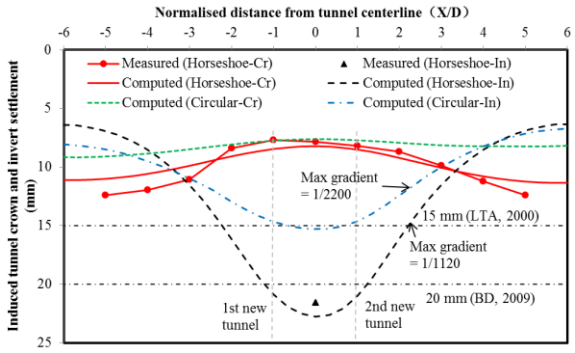

Fig. 5 Tunnel crown and invert settlements induced by twin-tunnel excavation

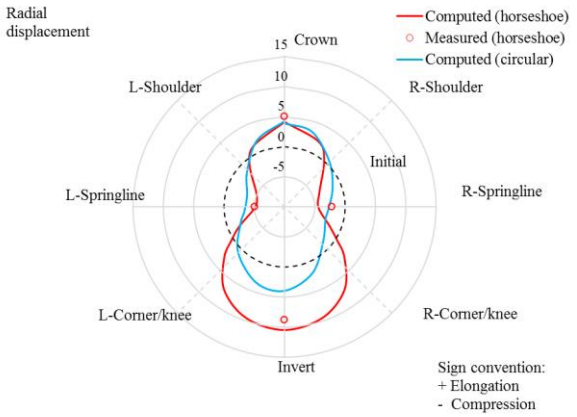

Fig. 6 Radial deformations of existing tunnel at X/D = 0 induced by twin-tunnel excavations

this section since test 2 is essentially the back-analyses of centrifuge test. However, only the computed result will be used for comparison. The measured results were plotted for validation of numerical model.

4.2 Shape effect on crown and invert settlements of existing tunnel due to twin-tunnel excavation (VL =1.5%)

Fig. 5 shows the crown and invert settlements of existing tunnel along longitudinal direction (X) after both new tunnels were excavated. There is only one measured data point for invert settlement because it can be deduced by adding crown settlement and tunnel vertical deformation, and only one set of potentiometers was installed at the midline (i.e., X/D=0) of the existing tunnel. Similar trends of settlement curve were observed for horseshoe and circular existing tunnel. In both cases, tunnel invert settled more than tunnel crown at the middle while less near the boundary, indicating that the existing tunnel was vertically elongated at the midline while compressed at the end in both cases. The crown settlement of circular existing tunnel was 7% smaller than that of horseshoe shaped tunnel at the middle (i.e., 7.6 and 8.2 mm). The farther away from the midline, the larger difference of tunnel crown settlement between two cases (up to 30%).

On the invert, significant difference was found in the invert settlement between two cases. The maximum invert settlement was 22.8 and 15.3 mm at midline (X/D=0) for horseshoe and circular existing tunnel, respectively, and gradually reduced to 5.6 and 6.9 mm at end of tunnel (X/D=6). The horseshoe shaped tunnel invert settled 29% more at midline while 19% less at the end than circular tunnel.

The maximum invert settlement of horseshoe shaped tunnel exceeded the limit of 15mm (LTA 2000) and 20 mm (BD 2009) while that of circular tunnel only exceeded standard of 15 mm (LTA 2000) by 2%. Moreover, the maximum gradient of invert settlement in horseshoe shaped tunnel was 1:1120 (close to the allowable limit of 1:1000 (BD 2009, LTA 2000), which was about twice of that in circular case (1:2200), both were located at a distance of 2.5 D from the midline of existing tunnel (i.e., X/D=2.5).

4.3 Radial deformation of existing tunnel with different shapes at X/D=0 (VL =1.5%)

Fig. 6 compares the radial deformation of existing tunnel between two numerical cases: horseshoe shaped existing tunnel and circular existing tunnel. The section X/D = 0 (middle of existing tunnel) was selected. The positive and negative signs denote elongation and compression in radial direction, respectively. Distortion of existing tunnel was observed in both cases. The deformed shape of existing tunnels rotated a little (about 10°) in clockwise direction. This is reasonable since soil is nonlinear material. The earlier excavated section 1-3 (as shown in Fig. 2(b)) would definitely cause distinct radial deformation of existing tunnel compared with those caused by section 4-6. Therefore, the deformed shape is asymmetric.

In horseshoe shaped existing tunnel case, the measured radial deformation at crown, invert, L-springlines and R-springline were 4, 10.5, -5.1 and -4.4 mm, respectively, indicating that tunnel was elongated in vertical direction while compressed in horizontal direction. In circular case, vertical elongation and horizontal compression were also observed. At the crown, elongation of tunnel (3.8 mm) was close to that in horseshoe case. At left and right springlines, the computed compressions were -3.4 and -2.8 mm, respectively, which were 33% and 36% less than those in horseshoe case. Furthermore, the elongation at invert in circular case (4 mm) was less than half of the value in horseshoe case. Noted that circular existing tunnel was designed to have identical sectional modulus, thickness and depth as the horseshoe shaped existing tunnel, the huge difference of radial deformation (45% smaller in vertical elongation, 33% smaller in horizontal compression) between two cases implies that horseshoe shaped tunnel is easier to deform. The explanation of this will be given in next section.

4.4 Shape effect on induced transverse bending strain and shear stress at X/D=0 (VL =1.5%)

Fig. 7(a) shows the induced bending strains of existing tunnel in transverse direction after twin-tunnel excavation. The bending strain is defined as transverse bending moment induced strain of tunnel lining, which is calculated from the

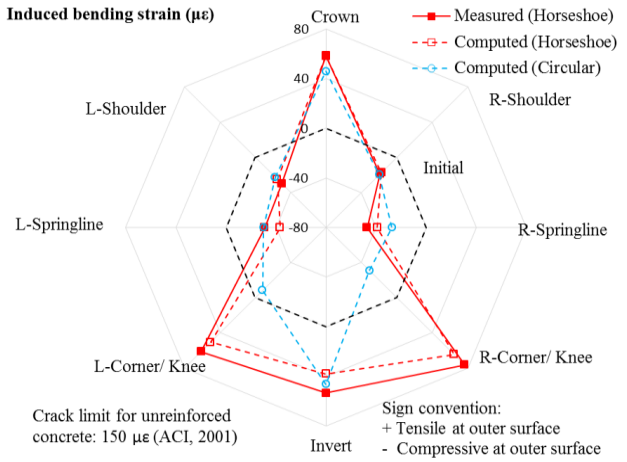

(a) Twin-tunnel excavation induced bending strain

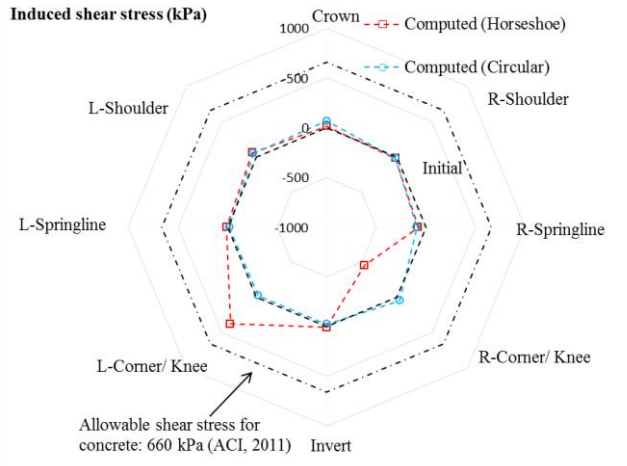

(b) Twin-tunnel excavation induced shear stress

Fig. 7 Existing tunnel's response along transverse direction at X/D=0

theoretical formula (i.e., ε=Mt/2EI). The positive and negative signs denote tensile and compressive strains at outer surface, respectively. There were some discrepancies between computed and measured results in terms of magnitude (within 20%). However, the trend of computed results shows a good match with measured ones. In both cases (computed and measured), positive bending strain occurred at crown and invert while negative bending strain was induced at both springlines. This is consistent with the previous results that the existing horseshoe shaped tunnel was vertically elongated and horizontally compressed.

At crown, L-sh (i.e., left shoulder) and R-sh (i.e., right shoulder), the induced bending strains in circular cases were 45.7, -22.5 and -19.8 με, which were slightly small than those of horseshoe (58, -25 and -17.5 με). This can explain why the crown elongation of circular case was slightly small than that of horseshoe case. At L-Sp (i.e., left springline) and R-Sp (i.e., right springline), induced bending strains in circular tunnel were -30.2 and -27.4 με, respectively, which were 30% less than the values in horseshoe shaped tunnel (-43.3 and -39.2 με). This is also consistent with the 33% less horizontal compression in circular tunnel compared with horseshoe case. At the invert, the induced bending strain of circular tunnel was 46.1 με, which is 22% larger than that in horseshoe shaped tunnel (37.7 με). However, the induced bending strains at left and right corners of horseshoe shaped tunnel were 50.4 and 64.5 με, respectively. This indicates that the bending strain maintained high positive value along the bottom plate of horseshoe shaped tunnel, maximum bending strain was located at two corners. Assuming the bottom part of horseshoe shaped tunnel as a beam, high positive bending strain along the bottom plate would cause large deflection. Comparing with the low (even negative) bending strain distributed on the lower part of circular tunnel, it is understandable why the invert elongation in horseshoe shaped tunnel is much larger than that in circular tunnel.

Fig. 7(b) shows the induced shear stresses along transverse direction. In circular tunnel, the magnitude of induced shear stresses was small (within ±100 kPa). The maximum induced shear stress (in absolute value) was -94 kPa, located at R-sh. For horseshoe shaped tunnel, the shear stresses were also negligible at crown, invert, both shoulders and both springlines. However, at left corner and right corner, substantial shear stresses (372 and -459 kPa) were mobilized, which were about four times the maximum value in circular case. The reason for this is that the axial stress cannot transfer continuously due to the 90° of turning angle at the two corners. As a result, large amount of shear force should be mobilized at the axillary angles to equalize the axial stress. Nevertheless, the shear stresses in two cases were both within the allowable shear stress limit for concrete of 660 kPa (ACI 2011). The tunnel lining's axial stress in transverse direction was not plotted since the incremental value is too small compared with its original value before excavation.

In summary, at the upper part of existing tunnel (i.e. crown and shoulders), the distribution and magnitude of bending strain and shear stress were quite similar in circular and horseshoe cases. At the middle part (i.e., springline) and lower part (i.e. invert and knees/corners), they differed a lot between two cases. In addition, substantial shear strain was mobilized around axillary angles of horseshoe shaped tunnel in relative to that in circular tunnel case. The explanations of the dissimilarities between circular and horseshoe cases are given as follows: (i) the upper part of horseshoe shaped tunnel was semicircle, which is identical to circular tunnel, thus stress in soil can transfer in similar path with similar magnitude. This resulted in that bending strain distribution in this part was similar between two cases. Moreover, hoop axial stress can transfer continuously in tunnel lining, therefore small amount of shear stress was mobilized; (ii) significant shear stress would be mobilized around axillary angles of horseshoe shaped existing tunnel because of its sectional geometry. The bending moment, which is the integration of shear stress, would be enlarged in semi-rectangle part of horseshoe shaped tunnel.

Such distinct internal force distribution between two cases can explain why radial deformation of horseshoe shaped existing tunnel is much larger than that of circular existing tunnel. On the other hand, the different shape of existing tunnel would affect the soil stress redistribution mechanism in surrounding soil. Therefore, it is also

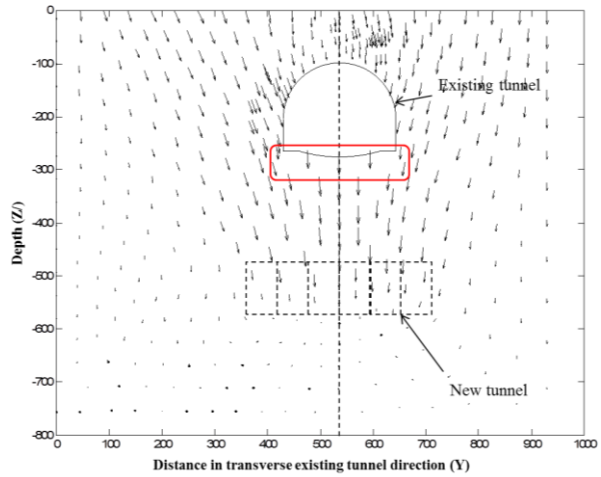

(a) Horseshoe shaped existing tunnel case

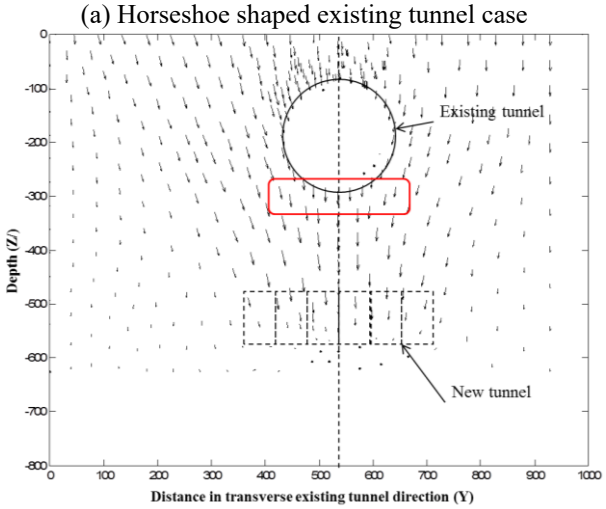

(b) circular existing tunnel case

Fig. 8 Tunneling induced soil displacement

meaningful to take a look at the soil disturbance of two cases for a better understanding of shape effect on multiple tunnel interaction.

4.5 Influence of tunnel shapes on soil displacement around existing tunnel at X/D = 0 (VL =1.5%)

Figs. 8(a) and 8(b) show soil displacement at the section X/D = 0 due to twin-tunnel excavation in horseshoe shaped tunnel case and circular tunnel case, respectively. The length and direction of arrows represent the magnitude and direction of soil displacement, respectively. In both cases, soil around existing tunnel moves downward and inward (i.e., towards the midline of new tunnel). This is due to the tunneling induced ground loss. The difference of soil displacement between two cases is mainly concentrated in the area underneath the existing tunnel (corresponding to the area in rectangular region). It is observed that the soil displacement in this area of horseshoe case is larger than that in circular case, which is consistent with the invert settlement result.

Another major difference of soil displacement between two cases is the direction of vectors underneath the existing tunnel. In this region, the directions of soil displacement in horseshoe shaped existing tunnel case are almost vertical. The tilting angels of vectors are relatively small (less than 10°). However, the tilting angles in the same region of circular case are larger compared with horseshoe case (about 15°). The horizontal component of soil displacement underneath the circular existing tunnel is larger compared with that in horseshoe case. The reason for this could also be attributed to the different tunnel shapes. The horizontal soil movement around the horseshoe shaped existing tunnel was greatly restricted by the side wall of existing tunnel. Therefore, vertical component of soil displacement is more dominant in horseshoe shaped existing tunnel case.

5. Effect of tunnel stiffness on multi-tunnel interactions

Fig. 9(a) shows relationship between radial deformation and stiffness of existing tunnel. The variation of tunnel stiffness was achieved by change the Young's modulus of existing tunnel lining. In total, three values of Young's modulus were simulated (i.e., 30, 69 and 150 GPa). The equivalent diameter and thickness of tunnel lining in concrete could be back-calculated with the given stiffness (i.e., flexural stiffness in longitudinal and transverse direction) modeled in this study. The positive and negative signs denote elongation and compression respectively. It is illustrated that with different Young's modulus of existing tunnel, the diameter changes (i.e., both in vertical and horizontal) of circular existing tunnel were always smaller than those of horseshoe existing tunnels. This further confirmed the postulation in previous section that horseshoe shaped tunnel is easier to deform than circular tunnel in both vertical and horizontal direction. With the increase of tunnel stiffness, the tunnel radial deformation decreased since tunnel had higher resistance against deformation. When Young's modulus of existing tunnel was increased from 30 GPa to 150 GPa, the radial deformation in vertical and horizontal direction decreased 15% and 14% in horseshoe shaped tunnel case, respectively. For circular tunnel case, vertical and horizontal diameter change decreased by 25% and 21% with same amount of increase in tunnel stiffness, respectively. This indicated that strengthening the existing tunnel's stiffness can enhance the tunnel's resistance against radial deformation more, especially for circular case. This is because the different deformation mechanism of circular and horseshoe shaped tunnel. Circular tunnel resisted the radial deformation mainly by its compressive stiffness. However, the resistance to radial deformation for horseshoe shaped tunnel was mainly owing to its flexural stiffness (i.e., bending stiffness). Thus, the resistance of circular tunnel to radial deformation is more sensitive to the material property (e.g., Young's modulus) rather than the sectional property (e.g., span of bottom plate). An optimization of dimensions (shape, size and thickness) of existing tunnel might be a better solution to reduce the radial deformation of horseshoe shaped tunnel rather than merely enhancing its Young's modulus.

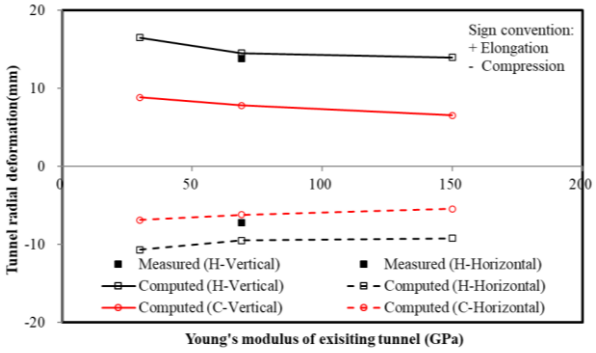

(a) Radial deformation of existing tunnel at X/D = 0

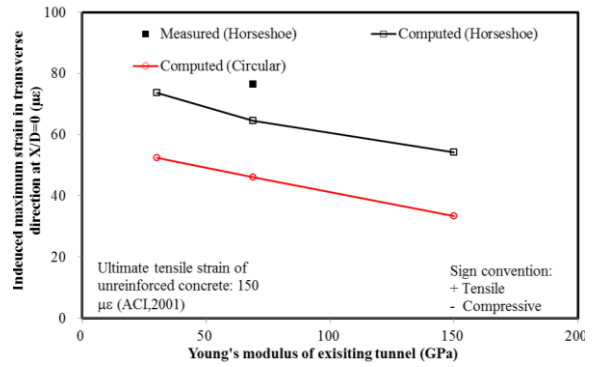

(b) Induced maximum bending strain in transverse direction at X/D =0

Fig. 9 Effect of tunnel stiffness on tunnel responses

Fig. 9(b) shows the induced maximum transverse bending strain of existing tunnel at X/D = 0 versus adopted Young's modulus of existing tunnel. As described in previous section (see Fig. 7(a)), maximum induced bending strain was located at invert and corner for the circular tunnel and horseshoe shaped tunnel, respectively. Therefore, in this section, only the maximum strains in two cases were plotted and discussed. The measured maximum bending strain of horseshoe shaped existing tunnel was 76.4 με while computed value was 64.5 με. The discrepancy of 15.5% is relatively acceptable which is maybe due to the experimental and calculation error. Since the transverse flexural stiffness of tunnel lining was proportional to the Young's modulus, bending strain is inversely proportional to Young's modulus. For both cases, the maximum bending strain decreased with increasing Young's modulus. By increasing tunnel stiffness from 30 GPa to 150 GPa, the maximum induced bending strain deceased by up 36%. The reason why induced maximum bending strain didn't reduced by 5 times is probably because that the tunnel-soil relative stiffness increased. Therefore, larger proportion of stress relief in soil was undertaken by existing tunnel. Stiffening the tunnel with given geometry in this study might be uneconomic and inefficient to alleviate twin-tunnel excavations induced adverse effects on the existing tunnel. Moreover, the reducing rate of maximum transverse strain with variation of Young's modulus is higher in circular tunnel, corresponding to previous observation that the resistance to radial deformation increased faster in circular tunnel.

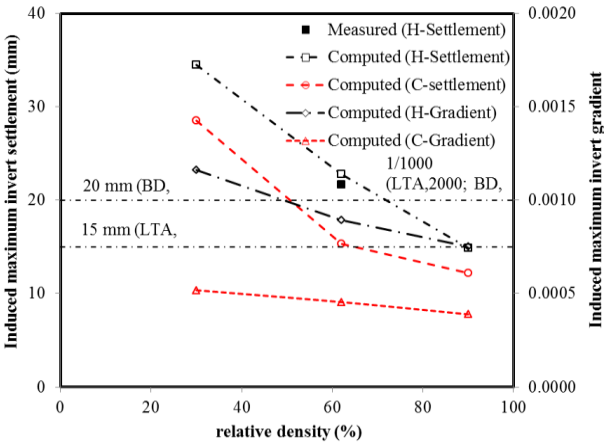

(a) Maximum tunnel invert settlement and gradient

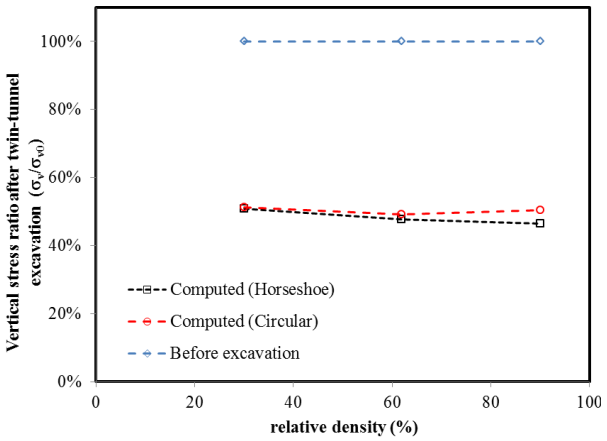

(b) Vertical soil stress ratio underneath existing tunnel invert

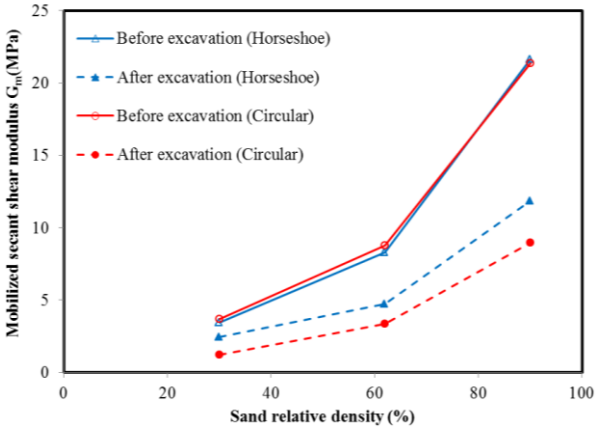

(c) Mobilized secant shear modulus underneath existing tunnel

Fig. 10 Effect of sand relative density on tunnel responses

6. Effect of relative density on tunnelling induced existing tunnel response

In this scenario, sand relative densities of 30%, 62% and 90%, corresponding to conditions of loose sand, medium dense sand and dense sand, were considered.

Fig. 10(a) shows relationships between induced maximum tunnel invert settlements and settlement gradients

with relative density (Dr). Since the sand with lower relative density has lower stiffness than the dense one, larger soil movement would be induced by new tunnel excavation in loose sand. As expected, it is observed that the induced maximum invert settlement decreased rapidly with the increase in relative density. The induced maximum invert settlement in the loose sand (i.e., Dr = 30%) were 131% and 133% larger than that in the dense sand (i.e., Dr = 90%) for horseshoe case and circular case, respectively. In addition, the maximum gradient for invert settlement increased by 54% and 33% with the decrease of relative density, respectively. When relative density was 30%, the maximum invert settlement of horseshoe and circular tunnel both exceeded the limit of 20 mm (BD 2009). Furthermore, the maximum settlement gradient in horseshoe shaped tunnel (1/860) also exceeded the allowable limit of 1/1000 (BD 2009, LTA 2000). When relative density reached 90%, the maximum invert settlement and gradient for both cases were all within the allowable limit (BD 2009, LTA 2000).

Fig. 10(b) shows the relationships between soil vertical stress ratio (ratio between vertical stress after twin-tunnel excavation with its original value, σ_v/σ_{vo}) beneath the existing tunnel invert and relative density. It is found that with the variation of relative density from 30% to 90%, the ratio of vertical stress relief ($1-\sigma_v/\sigma_{vo}$) of horseshoe shaped tunnel ranged from 49% to 53%. In circular case, the stress relief ratio ranged from 49% to 51%. It is illustrated that tunneling induced soil vertical stress relief underneath the circular existing tunnel is close to that underneath horseshoe shaped existing tunnel. Moreover, the vertical stress relief ratio is unrelated to the relative density.

Fig. 10(c) compares the mobilized secant shear modulus (G_m) of sand with different relative density. The mobilized secant shear modulus Gm was defined as $Gm = q/3\gamma s$, which can represent the stiffness of soil at current state. Prior to excavation of new tunnels, the secant shear modulus underneath existing tunnel in two cases (horseshoe and circular existing tunnel) were very close. This confirmed the repeatability of the numerical model conducted in this study. It is clearly demonstrated that relative density of sand significantly affects the stiffness of sand. By increasing Dr from 30% to 90%, the Gm increased by about 5 times before tunnel excavation. After the twin-tunnel excavations were completed, the Gm decreased by (30%-64%). This explains why invert settlement of existing tunnel increased by 130% with decrease of relative density. The reason for this stiffness degradation is that soil is stress and strain dependent material. The excavation would induce stress relief (further cause decrease in mean stress p') and mobilize shear strain, which both would reduce the stiffness of soil. Additionally, the stiffness degradation in circular tunnel case (60% - 64%) was larger than in horseshoe case (31%-46%). Since the ratios of stress relief underneath the existing tunnel in two cases were close, the difference in stiffness implied that the mobilized shear strain underneath the exisiting tunnel was larger in circular case. In another word, larger proportion of responses induced by new tunnel excavation (including soil responses and existing tunnel responses) were undertaken by the ground itself in circular case. A possible deduction of this fact is that the horseshoe shaped tunnel would cut off the transferring path for soil stress while circular tunnel wouldn't because of its smooth shape. Therefore, surrounding soil would interact with horseshoe shaped existing tunnel more than circular existing tunnel.

7. Conclusions

Three-dimensional numerical analyses had been conducted to investigate the effects of existing tunnel shape on multi-tunnel interaction. By conducting parametric studies on both cases with horseshoe shaped and circular existing tunnel, the following conclusions can be drawn:

(1) The value of volume loss plays the most important role in the multi-tunnel interactions. With each level of volume loss, settlement of horseshoe shaped existing tunnel is larger than circular existing tunnel's. Moreover, for the given geometry in this study, the maximum invert settlement and settlement gradient of horseshoe shaped existing tunnel exceeded the allowable limit by about 60% when induced volume loss is 2.5%. Countermeasures (e.g., grouting for shield tunnel) may be necessary to reduce the excessive tunnel settlement of horseshoe shaped tunnel induced by twin-tunnel excavation.

(2) In longitudinal direction, more serious serviceability issues (i.e., maximum tunnel settlement and gradient) would occur in horseshoe shaped tunnel due to twin-tunnel excavation than circular tunnel. The maximum invert settlement and gradient in horseshoe shaped existing tunnel case were 50% and 96% larger than those in circular tunnel case. This is mainly because of the larger vertical radial deformation of horseshoe shaped tunnel.

(3) In transverse section of existing tunnel at X/D=0, the vertical elongation and horizontal compression after twin-tunnel excavation in circular existing tunnel were 45% and 33% smaller than those in horseshoe case. This is attributed to the larger bending moment distribution in horseshoe shaped tunnel compared with circular tunnel. Since the hoop axial stress cannot transfer continuously at two axillary angles in horseshoe shaped tunnel, shear stress were mobilized to equalize the axial stress. As a result, huge amount of the bending moment occurred along the bottom plate of horseshoe shaped tunnel.

(4) The radial deformation of circular existing tunnel is more sensitive to the Young's modulus, which is because the different deformation mechanism of two different shapes. Circular tunnel resisted the radial deformation mainly by its compressive stiffness while horseshoe shaped tunnel do so mainly by its flexural rigidity. An optimization of dimensions of existing tunnel might be a better solution to reduce the radial deformation of horseshoe shaped tunnel rather than merely enhancing its material property or thickness.

(5) The induced invert settlement and settlement gradient of existing tunnel increased by up to 133% and 54% with the decrease of relative density of sand, respectively. This is because of that soil stiffness is highly related to its relative density. In addition, the reduction of soil stiffness beneath the circular tunnel was larger than that in horseshoe shaped tunnel, indicating that large portion of tunneling effect were undertaken by the ground itself in circular case.

Acknowledgments

The research described in this paper was financially supported by the Research and Development Plan in key Areas of Guangzhou (project number 20220602JBGS01).

References

ACI 224R-01 (2001), Control of cracking in concrete structures, American Concrete Institute; Farmington Hills, MI, USA.

ACI 318M-11 (2011), Building code requirements for structural concrete and commentary, American Concrete Institute; Farmington Hills, MI, USA.

Bai, X.D., Cheng, W.C. and Li, G. (2021), "A comparative study of different machine learning algorithms in predicting epb shield behaviour: a case study at the xi'an metro, china", *Acta Geotechnica*, (16-12). https://doi-org/10.1007/s11440-021-01383-7.

BD (2009), Technical notes for guidance in assessing the effects of civil engineering construction / building development on railway structures and operations, Building Department of the Government of HKSAR; HKSAR.

Boonyarak, T. and Ng, C.W. (2014), "Effects of construction sequence and cover depth on crossing-tunnel interaction", *Can. Geotech. J.*, **52**(999), 1-17. https://doi-org/ 10.1139/cgj-2014-0235.

Cooper, M.L., Chapman, D.N., Rogers, C.D.F. and Chan, A.H.C. (2002), "Movements in the Piccadilly Line tunnels due to the Heathrow Express construction", *Géotechnique*, **52**(4), 243-257. https://doi-org/10.1680/geot.52.4.243.41019.

Eskandari, F., Goharrizi, K.G. and Hooti, A. (2018), "The impact of epb pressure on surface settlement and face displacement in intersection of triple tunnels at mashhad metro", *Geomech. Eng.*, **15**(2), 769-774. https://doi-org/ 10.12989/gae.2018.15.2.769.

Fang, J.C., Kong, G.Q. and Yang, Q. (2022), "Group performance of energy piles under cyclic and variable thermal loading", *J. Geotech. Geoenviron. Eng.*, **148**(8), 04022060. https://doi-org/ 10.1061/(ASCE)GT.1943-5606.0002840.

González-Nicieza, C., Álvarez-Vigil, A.E., Menéndez-Díaz, A., and González-Palacio, C. (2008), "Influence of the depth and shape of a tunnel in the application of the convergence–confinement method", *Tunn. Undergr. Sp. Tech.*, **23**(1), 25-37. https://doi-org/ 10.1016/j.tust.2006.12.001.

Gudehus, G. and Mašín, D. (2009), "Graphical representation of constitutive equations", Géotechnique, **59**(2), 147-151. https://doi-org/ 10.1680/geot.2007.00155.

Hu, W., Cheng, W.C., Wen, S. and Yuan, K. (2021), "Revealing the enhancement and degradation mechanisms affecting the performance of carbonate precipitation in EICP process", *Front. Bioeng. Biotech.*, **9**, 750258. https://doi.org/10.3389/fbioe.2021.750258.

Jiang, B., Chen, L., Yang, J.S., Wang, S.Y. and Ng, C.W.W. (2017), "Effects of twin-tunnel excavation on an existing horseshoe-shaped tunnel considering the influence of a settlement joint", *Can. Geotech. J.*, 54. https://doi-org/ 10.1139/cgj-2015-0389.

Kim, S.H., Burd, H.J. and Milligan, G.W.E. (1998), "Model testing of closely spaced tunnels in clay", *Geotechnique*, **48**(3), 375-388. https://doi-org/ 10.1680/geot.1998.48.3.375.

Li, X.G. and Yuan, D.J. (2012), "Response of a double-decked metro tunnel to shield driving of twin closely under-crossing tunnels", *Tunn. Undergr. Sp. Tech.*, **28**, 18-30. https://doi-org/10.1016/j.tust.2011.08.005.

Liu, H.Y., Small, J.C., Carter, J.P. and Williams, D.J. (2009), "Effects of tunnelling on existing support systems of perpendicularly crossing tunnels", *Comput. Geotech.*, **36**(5), 880-894. https://doi-org/ 10.1016/j.compgeo.2009.01.013.

LTA (2009), Code of practice for railway protection, Development and Building Control Department, Land Transport Authority; Singapore.

Mishra, S., Zaid, M., Rao, K.S. and Gupta N.K. (2022), "FEA of urban rock tunnels under impact loading at targeted velocity", *Geotech. Geolo. Eng.*, **40**, 1693-1711. https://doi.org/10.1007/s10706-021-01987-6

Mohamad, H., Bennett, P.J., Soga, K., Mair, R.J. and Bowers, K. (2010), "Behaviour of an old masonry tunnel due to tunnelling-induced ground settlement", *Géotechnique*, **60**(12), 927-938. https://doi-org/10.1680/geot.8.P.074.

Mohamad, H., Soga, K., Bennett, P.J., Mair, R.J. and Lim, C.S. (2012), "Monitoring twin tunnel interaction using distributed optical fiber strain measurements", *J. Geotech. Geoenviron. Eng.*, **138**(8), 957-967. https://doi-org/10.1061/(ASCE)GT.1943-5606.0000656.

Nawel, B. and Salah, M. (2015), "Numerical modeling of two parallel tunnels interaction using three-dimensional finite elements method", *Geomech. Eng.*, **9**(6), 775-791. https://doi-org/ 10.12989/gae.2015.9.6.775.

Ng, C.W.W. (2014), "The state-of-the-art centrifuge modelling of geotechnical problems at HKUST", *J. Zhejiang University-Science A(Applied Physics & Engineering)*, **15**(1), 1-21. https://doi-org/ 10.1631/jzus.A1300217.

Ng, C.W., Boonyarak, T. and Mašín, D. (2013), "Three-dimensional centrifuge and numerical modeling of the interaction between perpendicularly crossing tunnels", *Can. Geotech. J.*, **50**(9), 935-946. https://doi-org/ 10.1139/cgj-2012-0445.

Ng, C.W., Boonyarak, T. and Mašín, D. (2015), "Effects of pillar depth and shielding on the interaction of crossing multitunnels", *J. Geotech. Geoenviron. Eng.*, **141**(6), 04015021. https://doi-org/ 10.1061/(ASCE)GT.1943-5606.0001293.

Ng, C.W.W., Shi, J.W. and Hong, Y. (2013), "Three-dimensional centrifuge modelling of basement excavation effects on an existing tunnel in dry sand", *Can. Geotech. J.*, **50**(8), 874-888. https://doi.org/10.1139/cgj-2012-0423.

Ng, C.W.W., Simons, N. and Menzies, B. (2004), "Soil-structure engineering of deep foundations, excavations and tunnels", Publisher: Thomas Telford, UK. ISBN: 0-7277-3263-3. 424p. 3rd re-print.

Ng, C.W.W., Xu, J. and Yung, S.Y. (2009), "Effects of wetting-drying and stress ratio on anisotropic stiffness of an unsaturated soil at very small strains", *Can. Geotech. J.*, **46**(9), 1062-1076. https://doi.org/10.1139/T09-043.

Niemunis, A. and Herle, I. (1997), "Hypoplastic model for cohesionless soils with elastic strain range", *Mech. Cohesive-frictional Mater.*, **2**(4), 279-299. https://doi.org/10.1002/(SICI)1099-1484(199710)2:4<279::AID-CFM29>3.0.CO;2-8.

Sadique, M.R., Zaid, M. and Alam, M.M. (2022), "Rock tunnel performance under blast loading through finite element analysis", *Geotech. Geol. Eng.*, **40**, 35-56. https://doi.org/10.1007/s10706-021-01879-9.

Shi, C. and Wang, Y. (2021). "Smart determination of borehole number and locations for stability analysis of multi-layered slopes using multiple point statistics and information entropy", *Can. Geotech. J.*, **58**(11), 1669-1689. https://doi.org/10.1139/cgj-2020-0327.

Shi, J.W., Fu, Z.Z. and Guo, W.L. (2019), "Investigation of geometric effects on three-dimensional tunnel deformation mechanisms due to basement excavation", *Comput. Geotech.*, **106**, 108-116. https://doi.org/10.1016/j.compgeo. 2018.10.019.

Shi, J.W., Ng, C.W.W. and Chen, Y.H. (2015), "Three-dimensional

numerical parametric study of the influence of basement excavation on existing tunnel", *Comput. Geotech.*, **63**, 146-158. https://doi.org/ 10.1016/j.compgeo.2014.09.002.

Shi, J.W., Zhang, X., Chen, Y. and Chen, L. (2018), "Numerical parametric study of countermeasures to alleviate basement excavation effects on an existing tunnel", *Tunn. Undergr. Sp. Tech.*, **72**, 145-153. https://doi.org/10.1016/j.tust.2017.11.030.

Shi, J.W., Ding C., Ng, C.W.W., Lu, H. and Chen L. (2020), "Effects of overconsolidation ratio on tunnel responses due to overlying basement excavation in clay", *Tunn. Undergr. Sp. Tech.*, **7**, 103247. https://doi.org/10.1016/j.tust.2019.103247.

Shi, J.W., Chen Y.H., Lu, H., Ma, S.K. and Ng, C.W.W. (2022a), "Centrifuge modeling of the influence of joint stiffness on pipeline response to underneath tunnel excavation", *Can. Geotech. J.*, **59**(9), 1568-1586. https://doi.org/10.1139/cgj-2020-0360.

Shi, J., Wei, J., Ng, C.W.W., Ma, S.K., Shi, C. and Li, P. (2022b), "Effects of construction sequence of double basement excavations on an existing floating pile", T*unn. Undergr. Sp. Tech*., **119**, 104230. https://doi.org/10.1016/j.tust.2021.104230.

Von Wolffersdorff, P.A. (1996), "A hypoplastic relation for granular materials with a predefined limit state surface", *Mech. Cohesive-frictional Mater*., **1**(3), 251-271. https://doi.org/10.1002/(SICI)1099-1484(199607)1:3<251 ::AID-CFM13>3.0.CO;2-3.

Wang, L., Cheng, W.C. and Xue, Z.F. (2022), "Investigating microscale structural characteristics and resultant macroscale mechanical properties of loess exposed to alkaline and saline environments", *Bull. Eng. Geol. Environ*., **81**(4), 1-17. https://doi.org/ 10.3389/fbioe.2021.750258.

Wang, Y., Shi, C. and Li, X. (2022), "Machine learning of geological details from borehole logs for development of high-resolution subsurface geological cross-section and geotechnical analysis", *Georisk*, **16**(1), 2-20. https://doi.org/10.1080/17499518.2021.1971254.

Yoo, C. and Cui, S.S. (2020), "Effect of new tunnel construction on structural performance of existing tunnel lining", *Geomech. Eng*., **22**(6), 497-507. https://doi-org/ 10.12989/gae.2020.22.6.497.

Zaid, M. (2021), "Dynamic stability analysis of rock tunnels subjected to impact loading with varying UCS", *Geomech. Eng*., **24**(6), 505-518. https://doi.org/10.12989/gae.2021.24.6.505.

Zaid, M. (2021), "Three-dimensional finite element analysis of urban rock tunnel under static loading condition: effect of the rock weathering", *Geomech. Eng*., **25**(2), 99-109. https://doi.org/10.12989/gae.2021.25.2.099.

Zaid, M. (2021), "Preliminary study to understand the effect of impact loading and rock weathering in tunnel constructed in quartzite", *Geotech. Geol. Eng*., https://doi.org/10.1007/s10706-021-01948-z.

Zaid, M. and Mishra, S. (2021), "Numerical analysis of shallow tunnels under static loading: a finite element approach", *Geotech. Geol. Eng*., **39**(3), 2581-2607. https://doi.org/10.1007/s10706-020-01647-1.

Zaid, M. and Shah, I.A. (2021), "Numerical analysis of Himalayan rock tunnels under xtatic and blast loading", *Geotech. Geol. Eng.*, **39**, 5063–5083. https://doi.org/10.1007/s10706-021-01813-z.

Zaid, M., Sadique, M.R. and Alam, M.M. (2022), "Blast resistant analysis of rock tunnel using abaqus: Effect of weathering", *Geotech. Geol. Eng*., **40**, 809–832. https://doi.org/10.1007/s10706-021-01927-4.